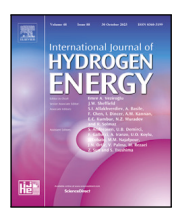
S S C C ELSEVIER

Contents lists available at ScienceDirect

# International Journal of Hydrogen Energy

journal homepage: www.elsevier.com/locate/he





# Experimental validation of DC-link based voltage control framework for islanded hydrogen DC microgrids<sup>†</sup>

Md Alamgir Hossain \*\*

School of Engineering, University of Southern Queensland, Toowoomba, 4350, Australia Blue Economy Cooperative Research Centre Ltd, Newnham Campus, Launceston, 7248, Australia The School of Engineering and Built Environment, Griffith University, Nathan, 4111, Australia

# ARTICLE INFO

# Keywords: Hydrogen microgrid Fuel cells Electrolysers Voltage controller Renewable energy integration DC power supply

# ABSTRACT

The integration of hydrogen technologies into islanded DC microgrids presents significant challenges in maintaining voltage stability and coordinating power flow under highly variable renewable energy conditions. This paper proposes a novel DC-link voltage control (DCVC) framework that incorporates adaptive droop control and autonomous operation algorithms to regulate fuel cells, electrolysers, and battery systems in a coordinated manner. Unlike conventional fixed-gain or priority-based methods, the proposed adaptive control dynamically adjusts the droop coefficient in response to voltage deviations, enhancing system stability and responsiveness. The control framework is validated on an industry-standard hydrogen DC microgrid platform developed at Griffith University, featuring real-time implementation on a Raspberry Pi controller and comprehensive integration with solar, wind, wave, and hydrogen energy sources. A small-signal stability analysis confirms that the proposed control ensures asymptotic voltage convergence under dynamic operating conditions. Experimental results across five case studies demonstrate that the proposed DCVC strategy ensures fast transient response, minimises overshoot, and maintains the DC-link voltage near the nominal 380 V under varying load and generation scenarios. The framework facilitates flexible energy sharing while ensuring safe hydrogen production and storage. It is also compatible with low-cost, open-source hardware, making it a scalable solution for remote and off-grid energy applications.

#### 1. Introduction

In the contemporary power system, the increasing emphasis on sustainable and renewable energy sources is reshaping the traditional landscape. The integration of renewable energy sources, such as solar and wind, presents both opportunities and challenges for the existing power infrastructure [1]. While the promise of cleaner energy and reduced environmental impact is evident, the intermittent nature of renewables introduces complexities in balancing supply and demand, grid stability, and overall reliability [2]. Moreover, managing energy flows within the microgrid, especially with fluctuating renewable energy inputs, requires sophisticated control algorithms to maintain grid stability. These challenges necessitate innovative solutions to ensure a smooth transition to a more sustainable energy paradigm.

One transformative approach to address the challenges of renewable energy integration is the incorporation of hydrogen fuel cells and electrolysers within a DC environment for efficient and reliable operation [3]. Hydrogen technologies offer a versatile means of energy storage and conversion, allowing excess energy generated during peak

renewable periods to be efficiently stored as hydrogen. This stored hydrogen can then be utilised during low-generation periods, effectively bridging the gap between variable renewable output and consistent energy demand [4]. The integration of hydrogen fuel cells and electrolysers in a power grid introduces a dynamic and adaptive energy storage solution, providing grid operators with greater flexibility and resilience in managing the inherent fluctuations associated with renewable energy sources [5]. These integrated technologies also gained popularity in microgrid applications, such as DC microgrids on ships or off-grid communities, where transportation of diesel is problematic and is not environmentally friendly due to greenhouse gas emissions. This provides a cost-effective solution to enhance power generation by harnessing locally derived renewable energy sources, mitigating their inherent variability [6]. However, producing and storing hydrogen efficiently for use in fuel cells or other applications presents a significant challenge, including electrolysers must operate dynamically, matching fluctuating energy inputs and demands while ensuring the safe and reliable storage of hydrogen.

This article is part of a Special issue entitled: 'Integrated Energy Solutions (Javani)' published in International Journal of Hydrogen Energy.

<sup>\*</sup> Correspondence to: School of Engineering, University of Southern Queensland, Toowoomba, 4350, Australia *E-mail addresses*: mdalamgir.hossain@unisq.edu.au, alamgir\_duet@hotmail.com.

Nomenclature							
AC	Alternating Current						
BESS	Battery Energy Storage System						
BMS	Battery Management System						
CEMPC	Centralised Economic Model Predictive Control						
COE	Cost of Energy						
DC	Direct Current						
DCVC	DC Voltage Control						
DEMPC	Distributed Economic Model Predictive Control						
EBDC	EV-Based Decentralised Charging						
EE	Excess Energy						
EMS	Energy Management System						
EV	Electric Vehicle						
EZ.	Electrolyser						
FC	Fuel Cell						
GA	Genetic Algorithm						
HESS	Hybrid Energy Storage System						
HLC	High-Level Controller						
HRS	Hydrogen Refuelling Station						
IDA-PBC	Interconnection and Damping Assignment						
IDA-PBC	Passivity-Based Control						
LCE	Life Cycle Emissions						
LLC	Low-Level Controller						
LPSP	Loss of Power Supply Probability						
m-SDWOA	Modified Symbiotic Differential Whale Op-						
III-3DVVOIT	timisation Algorithm						
MG	Microgrid						
MH	Metal Hydride						
MILP	Mixed-Integer Linear Programming						
MINLP	Mixed-Integer Linear Programming Mixed-Integer Nonlinear Programming						
MPC	Mixed-Integer Nonlinear Programming  Model Predictive Control						
MPPT	Maximum Power Point Tracking						
NN	Neural Network						
OR	Operating Reserve						
PEM	Proton Exchange Membrane						
PI	Proton Exchange Membrane Proportional–Integral						
PMS							
PSO	Power Management Strategy Particle Swarm Optimisation						
PV	Photovoltaic						
RES							
Rpi							
SAC							
SMRC	•						
SoC	Renewable Energy Sources Raspberry Pi System Annual Cost Sliding Mode Reference Conditioning State of Charge (battery)						
Z-score	Standardised statistical measure used to						
Z-score	assess electricity price trends						
$\Delta V$	Voltage deviation (V)						
	Efficiency						
η	Battery charging efficiency						
$\eta_c$							
$\eta_d$	Battery discharging efficiency Solar panel conversion efficiency						
$\eta_s$	_						
$\eta_w v$	Wave generator efficiency						
$\eta_{ m elz}$	Electrolyser efficiency Fuel cell efficiency						
$\eta_{\mathrm{fc}}$	Angular frequency (rad/s)						
ω	Water density (kg/m <sup>3</sup> )						
ρ	water density (kg/III-)						

$\boldsymbol{A}$	Area of PV panels (m <sup>2</sup> )					
BL(t)	Battery energy level at time <i>t</i> (Wh)					
$BL_{max}$	Maximum allowable battery energy level (Wh)					
$BL_{min}$	Minimum allowable battery energy level (Wh)					
C	Capacitance (F)					
$D_{ m h2}$	Density of hydrogen at STP (kg/m <sup>3</sup> )					
DI	Decision Interval (s)					
$E_{ m h}$	Energy content of hydrogen (J/g)					
$E_{\mathrm{ip}}$	Input energy to electrolyser (kWh)					
$H_s^r$	Spectral significant wave height (m)					
$H_{2_{ m cr}}$	Hydrogen consumption rate (m <sup>3</sup> /s)					
$H_{2_{ m pr}}$	Hydrogen production rate (m <sup>3</sup> /s)					
$H_{2_{ m st,maxC}}$	Maximum hydrogen storage capacity (m <sup>3</sup> )					
$H_{2_{ m st,max}}$	Maximum hydrogen storage limit (m <sup>3</sup> )					
$H_{2_{ m st,min}}$	Minimum hydrogen storage limit (m³)					
$H_{2_{st,t+1}}$	Hydrogen storage level at time $t + 1$ (m <sup>3</sup> )					
$H_{2_{\text{st},t}}$	Hydrogen storage level at time $t$ (m <sup>3</sup> )					
$H_{\mathrm{2p}}^{^{2}\mathrm{st},t}$	Mass of produced hydrogen (kg)					
$H_{\mathrm{fr}}$	Hydrogen flow rate extracted for fuel cells					
11	(g/s)					
$H_{SOC}$	State of hydrogen storage					
$I_{ m dc}$	DC current (A)					
$K_i$	Integral gain					
$K_p$	Proportional gain					
$P_c(t)$	Battery charging power at time <i>t</i> (W)					
$P_d(t)$	Battery discharging power at time t (W)					
$P_r$	Rated power of wind turbine (W)					
$P_{s}$	Output power from a solar panel (W)					
$P_w$	Wind turbine output power (W)					
$P_{\rm bat}$	Battery charging/discharging power (W)					
$P_{\mathrm{EL}}$	Power consumed by electrolyser (W)					
$P_{\rm EZ}$	Electrolyser power (W)					
$P_{\rm FC}$	Fuel cell output power (W)					
$P_{\text{FC}}$	Power from fuel cell (W)					
$P_{\rm load}$	Load power (W)					
$P_{\rm PV}$	Power from PV panels (W) Fuel cell output power (W)					
$P_{\rm fc}$	Maximum battery charging power (W)					
$P_{c,\max}$	Maximum battery discharging power (W)					
$P_{d,\max}$ $P_{sT}$	Total solar power output (W)					
$P_{wT}$	Total wind power output (W)					
$P_{uv}$	Time-averaged wave power output (W)					
PH	Prediction Horizon (s)					
SI	Solar irradiation (W/m <sup>2</sup> )					
T	Temperature (° C)					
$T_E$	Mean energy period of wave (s)					
$t_o$	Outside air temperature (° C)					
$t_r$	Rise time (s)					
$t_s$	Settling time (s)					
$U_{ m h2}$	Energy density of hydrogen (kWh/kg)					
v	Wind speed (m/s)					
$v_c$	Cut-in wind speed (m/s)					
$v_f$	Cut-out wind speed (m/s)					
$v_r$	Rated wind speed (m/s)					
$V_{ m dc}$	DC-link voltage (V)					
$V_{ m ref}$	Reference DC voltage (V)					

$V_{ m h2}$	Volume of produced hydrogen (m <sup>3</sup> )
w	Absorber width of wave generator (m)
$V_{ m max}$	Maximum allowable voltage (V)
$V_{ m min}$	Minimum allowable voltage (V)

Several recent publications have investigated the resource configuration, design, and optimisation of hydrogen microgrids. For example, in [7], a renewable energy-based green hydrogen and oxygen production system for aquaculture was developed, highlighting the role of hydrogen in sustainable food production. The optimisation of hydrogen storage in hybrid renewable energy systems under economic and environmental uncertainties was explored in [8], showcasing strategies for balancing performance and cost. In transportation, a photovoltaic and wind turbine-powered hydrogen refuelling system was analysed in [9], leading to significant reductions in carbon intensity and levelised driving costs, further illustrating the economic and environmental benefits of hydrogen-based solutions. In [10], an economic model predictive control for an alkaline electrolyser in a multi-energy system is presented, with improved operational cost saving of 38% compared to a traditional economic strategy.

Advanced control strategies are also crucial for ensuring the reliable operation of hydrogen microgrids. A hierarchical model predictive control system was developed in [11] to integrate wind energy into a hydrogen storage system, optimising revenue and reducing operating costs. Similarly, an efficient hydrogen-energy storage system (HESS) management strategy in a wind-solar microgrid, addressing economic, operational, and degradation constraints, is presented in [12]. A hybrid energy storage system that combines batteries for short-term needs and hydrogen storage for long-term applications was presented in [13], utilising passivity-based control and sliding mode reference conditioning to ensure system stability. A lab-scale stand-alone hydrogen energy system using a predictive power management strategy is presented in [14] to optimise energy control, with a highlight of the importance of intelligent power management over rule-based systems. The work has been extended by comparing the impact of predictive and reactive power management strategy in [15], indicating that predictive outperforms reactive management strategies.

Further advancements include two-layer hierarchical control strategies [16], which combine primary interconnection and damping assignment passivity-based control with supervisory model predictive control to maintain power balance and enhance system stability. Distributed economic model predictive control, as explored in [17], reduces computational burdens while optimising energy management and DC link voltage stability in PV/hydrogen DC microgrids. Additionally, in [18], hydrogen storage as a financially viable alternative to batteries for high-power applications in Power-to-X systems is emphasised, further strengthening the case for hydrogen integration in renewable energy networks. In [19], a supervisory model for scheduling distributed hybrid energy system fuelling stations to track external hydrogen and electricity consumers is presented. An optimal scheduling approach for managing energy in a solar-hydrogen microgrid is discussed in [20], integrating solar panels, HESS, and Battery Energy Storage System (BESS) to meet both electrical and hydrogen demands of an industrial hydrogen facility. In [21], a control strategy for a grid-connected wind farm paired with hybrid energy storage is introduced, aiming to meet electrical and contractual demands while producing hydrogen as a fuel for fuel cell EVs. A summary of the reviewed literature is presented in Table 1, providing a comparative evaluation of recent advancements in control strategies, hydrogen modelling, and system-level validation in hydrogen-integrated microgrids.

Despite significant advances in hydrogen-based microgrids and renewable integration, several critical research gaps remain. Many existing studies rely heavily on simulation or hardware-in-the-loop (HIL)

test as shown in Table 1, which do not fully replicate the operational complexities of real-world systems. These approaches often overlook transient uncertainties and integration challenges associated with physical hydrogen components. Most prior works emphasise individual resource control or fixed-priority logic, lacking a unified and autonomous strategy to coordinate fuel cells, electrolysers, and battery systems in real time. Moreover, system models for hydrogen components are often idealised or assumed, leading to inaccurate controller tuning. Finally, the reliance on expensive, proprietary platforms limits the scalability and practical deployment of microgrid control systems in cost-sensitive, remote, or offshore environments.

This study addresses these challenges by proposing and experimentally validating a novel adaptive droop-based voltage control framework tailored for islanded hydrogen DC microgrids. The adaptive droop controller dynamically adjusts its gain in response to voltage deviations, enabling both fast transient recovery and stable steady-state performance. A fully autonomous control algorithm is developed to coordinate the operation of fuel cells, electrolysers, and batteries based on real-time system states such as voltage level and state-of-charge (SoC). Second-order dynamic models of the fuel cell and electrolyser systems are derived from experimental data, allowing for accurate control design and tuning. The proposed framework is implemented on a low-cost, open-source platform using Raspberry Pi, NodeRED, and Grafana, and validated through five hardware-based case studies. Results show reliable DC-link voltage regulation near 380 V, reduced overshoot, and improved response time under variable renewable inputs and load fluctuations. This work not only improves the control precision and resilience of hydrogen microgrids but also provides a scalable, cost-effective solution for real-world deployment in remote or off-grid applications such as aquaculture and islanded energy systems. The main contributions of this paper are summarised as follows:

A novel DC-link voltage control (DCVC) framework is developed for islanded hydrogen DC microgrids, incorporating adaptive droop controllers that dynamically tune the gain based on real-time voltage deviations to improve transient response and

tability.

 An autonomous control algorithm is proposed for seamless and coordinated operation of electrolysers, fuel cells, and battery banks based on voltage thresholds and SoC conditions, minimising reliance on centralised decision-making or fixed-priority logic.

- Second-order dynamic models of the fuel cell and electrolyser systems are experimentally derived and validated, capturing overshoot, damping, and settling behaviour critical for controller tuning and real-time implementation.
- The proposed control strategy is experimentally validated on a fully functional hydrogen DC microgrid platform built at Griffith University, using open-source software (NodeRED, Grafana) and low-cost Raspberry Pi hardware, demonstrating robust voltage stabilisation under fluctuating renewable inputs.
- A comprehensive small-signal stability analysis is performed, demonstrating that the combined droop gains from fuel cells, electrolysers, and battery systems result in a first-order differential voltage response with guaranteed asymptotic stability, thereby validating the robustness of the control framework under dynamic load and generation fluctuations.

The paper is organised as follows. Section 2 presents an application scenario and component modelling of a hydrogen DC microgrid in an aquaculture environment. The proposed voltage-based control framework is developed in Section 3 for the autonomous operation of the hydrogen microgrid with efficient operation. Section 4 carries out industry-standard experiments with five case studies to demonstrate the effectiveness of the proposed DCVC framework for microgrid reliable operation. The work is concluded in Section 5.

Table 1
Comparative summary of key literature and this work

Study	Focus area	Control strategy	Validation method	Hydrogen component	Hardware/Plat- form	Key limitation addressed
				modelling		
Ref. [7]	$H_2 + O_2$ for aquaculture	System-level RES–H <sub>2</sub> design	Case study sim. (5 cities)	Thermodynamic PEM EZ modelling	No real-time hardware	No automation; lacks experimental control
Ref. [8]	H <sub>2</sub> system under uncertainty	MILP-based robust EMS	Sim. in AIMMS	Static sizing with uncertainty	No hardware test	Ignores dynamics; lacks real-time control
Ref. [9]	HRS for buses	RDO optimisation	Uncertainty- based sim.	Sizing of PV/wind/HRS	Sim-only HRS model	Transport focus; lacks EMS detail
Ref. [10]	Solar-H <sub>2</sub> system for buildings	Harmony Search metaheuristic	Sim. using SAC, LPSP	Simplified tank and FC cost model	MATLAB sim. only	No real-time EMS or controller design
Ref. [11]	Wind-H <sub>2</sub> MG (grid+island)	Hierarchical MPC (HLC+LLC)	Sim. via MLD	HESS degradation and switching	Wind site; no controller yet	No HW test; validation pending
Ref. [12]	Islanded wind–solar MG + H <sub>2</sub> tanks	Cascaded MPC	Sim. + lab-scale	Tank selection via MLD	Lab MG; no low-cost controller	Complex logic; not scalable
Ref. [13]	DC MG with HRS logic	IDA-PBC + SMRC	Sim. only	Unified bidirectional conv. model	MATLAB only	No exp. system or real MG deployment
Ref. [14]	Standalone H <sub>2</sub> + MH storage	Predictive PMS (NN vs. rule-based)	Lab-scale validation	Implicit FC/storage modelling	Emulated RES, real FC	No scalable EMS; economic aspects missed
Ref. [15]	Wind-Batt-H <sub>2</sub> hybrid sizing impact	PMS + PSO + GA	Sim. with real profiles	FC/EZ transient incl.	MATLAB; FC data from lab	No embedded control; high-level analysis
Ref. [16]	DC MG w/ battery + H <sub>2</sub> storage	IDA-PBC + MPC (2-layer)	Sim. with loads/RES	Lyapunov-based nonlinear FC/EZ models	Simulink-based	No field deployment or embedded use
Ref. [17]	PV/H <sub>2</sub> DC MG EMS	DEMPC with local controllers	Sim. with MINLP solver	PV/FC/EZ + converter models	Simulation only	Switching losses ignored; no HW test
Ref. [18]	H <sub>2</sub> in P2X systems	m-SDWOA optimisation	Sim. vs WOA/PSO	DC-bus, EZ trends	Sim. (evo. algo toolkit)	No EMS/HW link; idealised behaviour
Ref. [19]	HRS for transport + OR services	Supervisory optimal scheduling	Sim. w/ hist. data	Dispatch models for FC/EZ	No HW; market model only	OR-centric; lacks microgrid dynamics
Ref. [20]	PV-BESS H <sub>2</sub> prod. EMS	Seasonal Z-score EMS	4-case study sim.	EZ efficiency + seasonal logic	MAT- LAB/Simulink	No controller implementation
Ref. [21]	Wind-integrated EV charging	MPC + EBDC (decentralised)	Sim. on multi-EV buildings	No H <sub>2</sub> components	Simulated decentralised nodes	EV-focused; not applicable to $H_2$ MGs
This Work	Islanded $H_2$ DC MG for aquaculture	Adaptive Droop + Autonomous	Five real-time experiments	2nd-order dynamic models (EZ, FC)	Raspberry Pi, Node-RED, Grafana, Python	Cost-effective, real-time, scalable, hardware-validated

# 2. Hydrogen DC microgrid

This study explores the renewable energy solutions in ocean environments through hydrogen DC microgrids envisioned to power an aquaculture facility, fostering environmental conservation and economic growth. The aquaculture industry plays a crucial role in addressing food availability and poverty, aligning with the United Nations Sustainable Development Goals [22]. The integration of a hydrogen microgrid exemplifies a promising solution to meet the energy needs of fish cultivation while minimising ecological impact. In this scenario, a remote coastal area with abundant access to ocean resources is chosen for its suitability for aquaculture activities, shown as indicative in Fig. 1. The components of the microgrid include offshore 1 kW of wind turbines, 1 kW of wave generators, 1 kW of fuel cells, 1.5 kW of electrolysers, 25.2 kWh of batteries, and 5 kW of solar panels on floating platforms to harness consistent energy from the ocean. These sources are connected to the microgrid through DC/DC power converter devices to ensure compatibility with the DC link voltage. A 25.2 kWh battery bank serves for short-term energy storage, while an electrolyser produces hydrogen for medium-to-long-term energy storage, facilitating grid resilience.

To facilitate power distribution and control, an advanced control system is designed in this study for power electronics devices. The controller utilises feedback control loops to adjust the power output and voltage levels of the electronic devices, which enable bidirectional power flow between the energy sources, storage systems, and loads, while ensuring voltage regulation within acceptable limits. Additionally, sensing and monitoring devices are deployed throughout the microgrid to provide real-time data on voltage, current, SoC, temperature and power flow, facilitating system analysis and performance evaluation. Data acquisition software platforms, such as NodeRed, Grafana and Python-based frameworks, are utilised for data logging, visualisation, and analysis. These activities are performed in a central controller. The supervisory software allows operators to remotely monitor system performance, adjust control parameters, and responds to system events in real-time, enhancing operational efficiency and reliability.

To enhance system robustness and avoid single points of failure, the DC microgrid is designed with three segmented battery banks, each rated at  $8.4~\mathrm{kWh}$  (configured as  $2.8~\mathrm{kWh}$   $\times 3$ ). This modular architecture ensures that in the event of a single battery bank failure, the

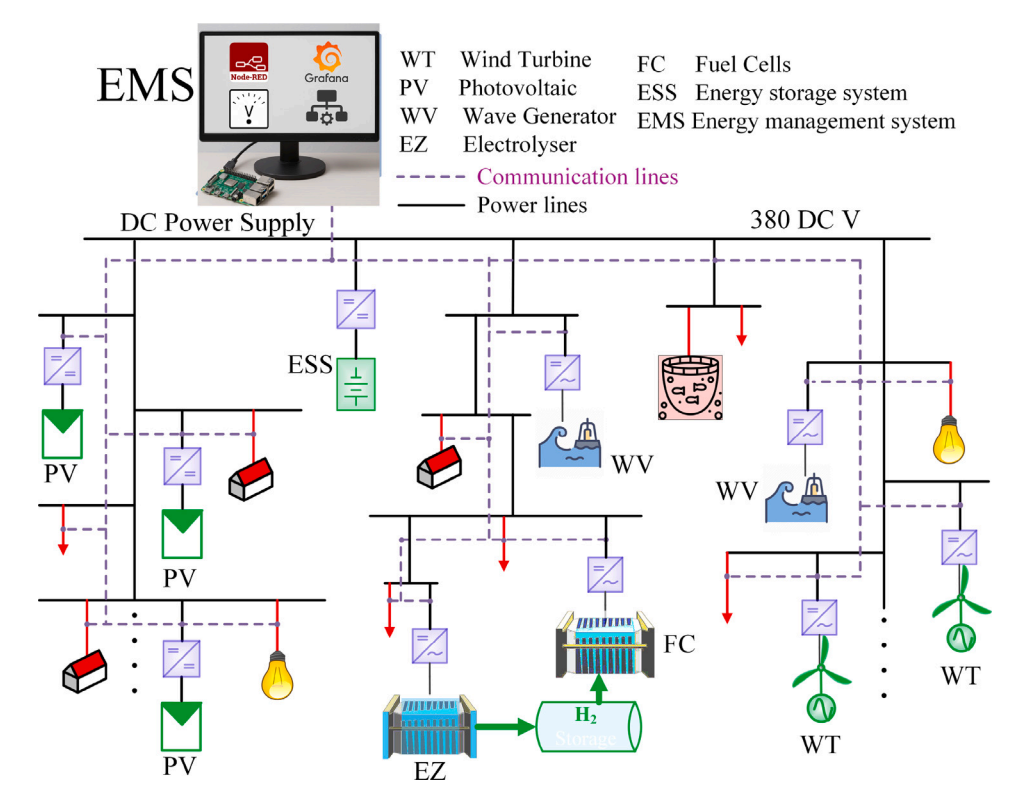


Fig. 1. Islanded Hydrogen DC Microgrid.

remaining banks can continue supporting critical operations without interrupting the power supply. The battery system functions as the backbone of the DC microgrid, ensuring stable voltage regulation and transient response. In addition, the control system includes comprehensive monitoring features through the Raspberry Pi controller, which continuously tracks the SoC or battery energy levels (BL(t)), voltage, temperature, and fault conditions across all energy storage units. To prevent unsafe conditions, the system has predefined upper and lower BL(t) thresholds, triggering alerts or automated shutdown when these are breached. If communication is lost or processor faults are detected, a watchdog timer mechanism initiates a fallback shutdown protocol, either handled manually via a central operating unit or automatically if limits are exceeded. Real-time data logging and fault flags ensure traceability, while ongoing monitoring of thermal and electrical parameters maintains operational safety and long-term system reliability.

The DC microgrid experimental platform for analysing ocean scenarios highlights the potential application of an islanded hydrogen DC microgrid in sustainable fish cultivation. The experimental results can also explore the amount of oxygen supply required for fish cultivation using the electrolyser. Ensuring an adequate oxygen supply is vital for the well-being and development of aquatic organisms, promoting optimal growth rates, reducing disease risks, and showcasing the responsible development of marine resources through the integration of renewable energy and aquaculture systems [23]. Submersible fish cages and cultivation infrastructure are designed for the specific ocean environment, promoting sustainable fish farming practices.

The modelling of various microgrid components used to emulate the practical scenarios for the experiment is presented as follows.

# 2.1. Solar generators

The output power from solar irradiation using solar panels, can be determined using the following equation [24]:

$$P_s = \eta_s \times A \times SI(1 - 0.005(t_o - 25)) \tag{1}$$

where  $\eta_s$  represents the conversion efficiency (in percentage), A is the area of PV panels (in m<sup>2</sup>), and  $t_o$  is the outside air temperature (in °C).

For a system with multiple solar panels, the total output power can be expressed as the sum of individual panel outputs:

$$P_{sT} = \sum_{n=1}^{N} P_{s,n} \tag{2}$$

where n (ranging from 1 to N) denotes the number of solar generators.

#### 2.2. Wind turbines

Wind power generation depends on wind velocities at the power rating and site of a wind turbine. The electric power as a piece-wise function of the wind speed is expressed as follows [24]:

$$P_{w} = \begin{cases} 0 & \text{if } v_{f} \leq v & \text{or } v \leq v_{c} \\ P_{r} \times \frac{v^{3} - v_{c}^{3}}{v_{r}^{3} - v_{c}^{3}} & \text{if } v_{c} < v < v_{r} \\ P_{r} & \text{if } v_{r} \leq v < v_{f} \end{cases}$$
(3)

where  $P_r$  is the rated electrical power in Watts,  $v_r$  is the rated wind speed in m/s, v represents wind speed,  $v_c$  is the cut-in wind speed, and  $v_f$  is the cut-off wind speed.

For a system with multiple wind turbines, the total output power can be calculated as follows:

$$P_{wT} = \sum_{i=1}^{J} P_{w,j} \tag{4}$$

where j (ranging from 1 to J) denotes the number of wind generators.

# 2.3. Wave generators

Wave generators harness ocean wave power through various mechanisms, making a universal performance model complex. A simplified expression for the time-averaged power output  $P_{wv}$  is given by [25]:

$$P_{wv} = \eta_{wv} \cdot w \cdot \rho \cdot H_s^2 \cdot T_E \tag{5}$$

where  $\eta_{wv}$  represents the efficiency of the absorber and power takeoff, w is the absorber size,  $\rho$  is the water density,  $H_s$  is the spectral significant wave height, and  $T_E$  denotes the mean energy period.

Due to the fluctuating nature of wave power, microgrid control strategies must account for its inherent variability. Mechanical and electrical smoothing techniques can mitigate fluctuations, but the power system must remain adaptable.

# 2.4. Storage systems

Battery energy levels for charging/discharging cycles can be represented as follows [24]:

$$BL(t) = BL(t-1) + \tau P_c(t)\eta_c$$
 if the battery is charged (6)

$$BL(t) = BL(t-1) + \tau P_d(t)/\eta_d$$
 if the battery is discharged (7)

subject to power limits:

$$0 < P_c(t) < P_{c,max}$$

$$P_{d max} < P_d(t) < 0$$

and battery energy level limits:

$$BL_{min} < BL(t) < BL_{max}$$

where  $P_c(t)$  is the charging power of the battery at time t,  $P_d(t)$  is the discharging power of the battery, BL(t) is the battery energy level,  $\tau$  is the time period interval, and  $\eta_c$  and  $\eta_d$  are the charging and discharging efficiencies, respectively.

#### 2.5. Fuel cells

Let  $H_{\rm fr}$  be the extracted hydrogen flow rate from the storage. The fuel cell power output ( $P_{\rm fc}$ ) is calculated using the following model:

$$P_{\rm fc} = \eta_{\rm fc} \times H_{\rm fr} \times E_{\rm h} \tag{8}$$

where  $\eta_{\rm fc}$  is the efficiency of the fuel cell (assumed to be 0.60),  $E_{\rm h}$  is energy content of hydrogen (assumed to be 237,000 J/g)

This generic model provides a representation of any fuel cell power generation based on the extracted hydrogen flow consumption. The model considers the efficiency of the fuel cell ( $\eta_{\rm fc}$ ) and the energy content of hydrogen ( $E_{\rm h}$ ), providing valuable insights into the power generation process.

# 2.6. Hydrogen electrolyser model

Let  $E_{\rm ip}$  be the energy input in kilowatt-hours (kWh),  $\eta_{\rm elz}$  be the efficiency of the electrolyser (assumed to be 70%),  $U_{\rm h2}$  be the energy density of hydrogen (33.33 kWh per kg of H<sub>2</sub>),  $D_{\rm h2}$  be the density of hydrogen at standard temperature and pressure (0.08988 kg per m³).

The mass of hydrogen produced  $(H_{2p})$  and its volume  $(V_{\rm h2})$  are calculated as follows:

$$H_{\rm 2p} = \frac{E_{\rm ip} \times \eta_{\rm elz}}{U_{\rm h2}} \tag{9}$$

$$V_{\rm h2} = \frac{H_{\rm 2p}}{D_{\rm h2}} \tag{10}$$

The hydrogen production rate  $(H_{\rm 2pr})$  is calculated based on the time interval  $(\tau)$ :

$$H_{\rm 2pr} = \frac{V_{\rm h2}}{\tau} \tag{11}$$

This generic model provides a representation of hydrogen production and flow rate based on the energy input and efficiency of an electrolyser. The model considers the energy density and density of hydrogen to quantify the produced mass and volume, and it calculates the production rate over a specified time interval.

#### 2.7. Hydrogen storage model

Let  $H_{2_{st,t+1}}$  be the storage level at time t+1,  $H_{2_{pr}}$  be the rate of hydrogen production from electrolysers,  $H_{2_{cr}}$  be the rate of hydrogen consumption by fuel cells,  $\tau$  be the time step in seconds, and  $H_{2_{st,max}C}$  be the maximum storage capacity.

The storage level  $(H_{2st,t+1})$  is updated based on the difference between the production rate and consumption rate over the time step:

$$H_{2_{st,t+1}} = H_{2_{st,t}} + (H_{2_{nr}} - H_{2_{cr}}) \times \tau \tag{12}$$

The storage level is then constrained not to exceed the maximum capacity or go below zero:

$$H_{2_{st,min}} < H_{2_{st}} < H_{2_{st,max}}$$

The maximum storage capacity  $(H_{2_{st,max}C})$  is assumed to be 1000 units of hydrogen.

This model provides a representation of hydrogen storage management based on production and consumption rates. The model ensures that the storage level is updated over time, considering the production and consumption dynamics, and it constrains the storage level within specified limits. To operate these components, in the next section, the dynamic voltage controllers are proposed.

#### 3. Proposed DCVC framework

This section proposes DCVC framework aimed at ensuring the smooth operation of the hydrogen DC microgrid. The framework consists of two aspects: voltage control to efficiently operate the hydrogen fuel cells and electrolyser; and algorithm development for autonomous operation of the microgrid without human interruption. The combination of the voltage control and algorithm development is presented as follows.

# 3.1. Voltage control

The focus is on dynamic control of hydrogen flow rates, and for this purpose, droop controls are introduced. These controls play a crucial role in regulating the electrolyser, fuel cell, and battery energy flow, ultimately enhancing the microgrid's resilience and reliability, especially during adverse weather conditions.

It is important to note that managing small-scale power generation and demand poses challenges due to the inherent high uncertainty in both generation and demand, particularly when compared to larger power networks. To address this complexity, a precisely designed control system is essential to prevent oscillations in the DC link voltage arising from unbalanced supply—demand issues [26]. The control system should effectively navigate the uncertainties to maintain stability and reliability in the microgrid's power distribution, ensuring a seamless and secure operation despite the dynamic and unpredictable nature of small-scale power generation and demand.

# 3.1.1. Dynamic hydrogen flow rate model

Let  $K_v$  be the droop coefficient,  $V_{\text{ref}}$  be the reference voltage, and  $V_{\text{dc}}(t)$  be the measured DC link voltage.

The hydrogen flow rate ( $H_{\rm fr}$ ) is calculated as follows:

$$H_{\rm fr} = K_v \cdot (V_{\rm ref} - V_{\rm dc}(t)) \tag{13}$$

This equation represents the linear relationship between the coefficient ( $K_v$ ), the difference between the reference voltage ( $V_{\rm ref}$ ), and the measured DC link voltage ( $V_{\rm dc}(t)$ ), providing a measure of the hydrogen flow rate that depends on power demands. This general Eq. (13) is used for both the operation of electrolyser and fuel cells, although the coefficient value will be different for both cases. For the electrolyser,  $K_v$  will be represented by  $K_{ez}$  and  $K_{fc}$  for the fuel cells.

$$K_{v}(t) = K_{v0} + \alpha \cdot |\Delta V(t)| \tag{14}$$

where:

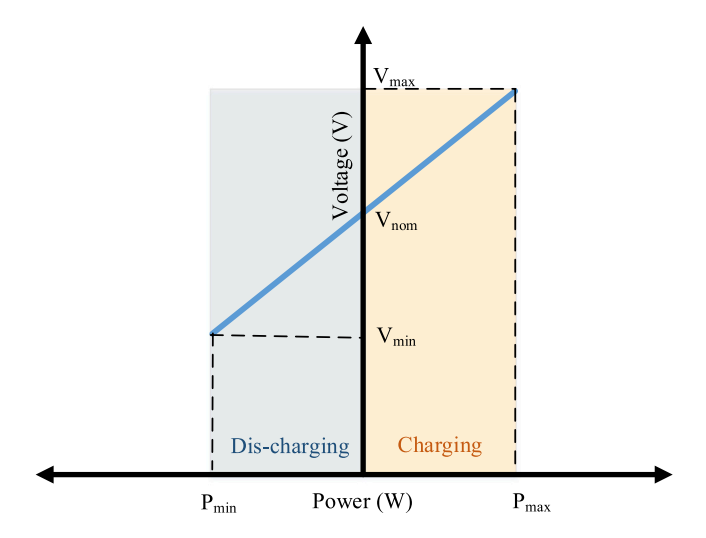


Fig. 2. Battery operational principles.

- $K_{v0}$  is the nominal base droop gain,
- $\alpha$  is the adaptive gain factor (tuning parameter),
- $|\Delta V(t)| = V_{\text{ref}} V_{\text{dc}}(t)$  is the magnitude of the voltage deviation, .

The parameter  $\alpha$  is chosen based on the maximum expected voltage deviation  $\Delta V_{\rm max}$  and the desired maximum gain  $K_{v,{\rm max}}$  using:

$$\alpha = \frac{K_{v,\text{max}} - K_{v0}}{\Delta V_{\text{max}}} \tag{15}$$

This ensures that the gain transitions smoothly from nominal to maximum over the operating voltage range.

The calculated hydrogen flow rate is then limited to the range [0, 0.0055] to ensure the physical feasibility of the power supply  $H_{\rm fr,\ min} < H_{\rm fr} < H_{\rm fr,\ max}$ . This constraint ensures that the hydrogen flow rate ( $H_{\rm fr}$ ) remains within the specified bounds.

# 3.1.2. Operating principle of fuel cells and electrolysers

For fuel cells, if DC link voltage is lower than the nominal voltage (380V), such as 370 V, then the highest capacity of hydrogen will flow to supply maximum power from the fuel cells for maintaining reliability and stability of the microgrid. In contrast, the lowest amount of hydrogen will flow if the DC link voltage is high, such as 375 V. This dynamic hydrogen flow is mapped through by designing droop control characteristics, whose slope is determined by physical constraints.

The rate of hydrogen production by an electrolyser depends on the power consumption. If the electrolyser consumes the highest capacity power, then the highest amount of hydrogen will be produced. To maintain DC link voltage within limits, the electrolyser has been operated by dynamic power consumption strategies. For low DC link voltage but higher in magnitudes,  $V_{dc}(t)$ , such as 385 V, low hydrogen is produced by consuming low power, whereas high hydrogen is produced by consuming the highest power consumption of electrolyser during the highest  $V_{dc}(t)$ , such as 390 V. By consuming more power during high renewable power generation, the electrolyser maintains a stable microgrid operation by regulating  $V_{dc}(t)$ .

# 3.1.3. Battery control strategy

The operation of the microgrid heavily relies on the battery bank, and its role is described by the battery droop coefficient  $(K_b)$ , a reference voltage, and measured DC link voltage. The power supplied by the battery  $(P_{\mathbf{b}}(t))$  is determined by the droop control equation:

$$P_{\mathbf{b}(t)} = \mathbf{K}_b \cdot (V_{\text{ref}} - V_{\text{dc}}(t)) \tag{16}$$

This equation governs the power adjustments required to regulate the DC link voltage ( $V_{dc}(t)$ ) towards the nominal voltage of 380 V. If

 $V_{
m dc}(t)$  surpasses  $V_{
m ref}$ ,  $P_{
m b}(t)$  becomes a negative value, signifying that the battery is charging to stabilise  $V_{dc}(t)$ . Conversely, the battery discharges when  $V_{
m dc}(t)$  is below  $V_{
m ref}$ , actively maintaining the nominal voltage in the DC link. The continuous charging and discharging cycles by the battery bank aim to sustain the nominal voltage, as depicted in Fig. 2. The battery bank is deemed the heart of the microgrid system, ensuring reliable, secure, and resilient operation.

The significance of the battery bank becomes evident in islanded areas where renewable energy sources generate power based on weather conditions. While fuel cells act as an independent source, their continuous operation is contingent on the availability of hydrogen. The microgrid's reliance on renewable energy and the intermittent nature of these sources underscores the critical role of the battery bank in maintaining stability.

Although the system integrates long-term storage through electrolyser and fuel cell systems, the battery bank plays a critical role in short-duration voltage regulation and fast transient suppression. Unlike hydrogen devices, batteries respond almost instantaneously to power imbalances, thereby stabilising the DC link during fast fluctuations and reducing stress on hydrogen components.

#### 3.2. Autonomous algorithm

The overall operational principle of the microgrid is centred around maximising power generation from renewable sources like solar PV, wind, and wave generators through maximum power point tracking. However, to ensure microgrid stability, especially during periods of over power generation when the battery is fully charged and the electrolyser operates at full capacity, power generation curtailment is implemented.

Key parameters guiding the flexible operation of the microgrid involve the combined working principle of hydrogen fuel cells, electrolyser, and battery operations. The operation is illustrated in Fig. 3, which provides a comprehensive view based on DC link voltage. The battery is continually active, either charging or discharging to maintain the DC link voltage close to the nominal voltage, 380 V. When  $V_{dc}(t)$  exceeds the nominal voltage, the electrolyser engages. In contrast, if it falls below the nominal voltage, fuel cells come into operation, supporting the DC link voltage within defined limits. This dynamic operation ensures stable microgrid performance in remote areas, simultaneously supplying oxygen for maintaining a healthy aquaculture fish cultivation and powering industries with zero-emission greenhouse gas emissions.

The algorithm of the microgrid is detailed in flowchart Fig. 4. To initiate the microgrid, the battery banks are first activated. If the BL(t) is outside the specified limit, the battery remains in standby mode, and the fuel cell charges the battery until the BL(t) is within the limit. If the battery energy level exceeds the minimum threshold, the battery operates using the proposed voltage control outlined in Eq. (16). Operating the microgrid during high BL(t) is permissible.

It is crucial to wait until the DC link voltage approaches the nominal voltage before activating renewable energy sources like solar PV, wind, and wave generators. Under these conditions, the microgrid is fully capable of maintaining a balance between power supply and demand. The  $V_{dc}(t)$  is continuously monitored, and if it experiences overvoltage, the electrolyser is activated; otherwise, the fuel cell is turned on during under voltage. The electrolyser operates according to the dynamic operation described in Eq. (13). It remains active as long as the  $V_{dc}(t)$  is within the specified range; otherwise, it is deactivated. Conversely, the fuel cells start operating as long as the  $V_{dc}(t)$  is within the acceptable range.

Once the microgrid is in operational mode, the fuel cells monitor the BL(t) status. If the BL(t) falls below the minimum threshold, the fuel cells supply power to the loads and charge the battery. If the battery BL(t) reaches its maximum capacity, the power from renewable energy sources is curtailed to ensure microgrid stability. This systematic approach ensures the reliable and secure operation of the microgrid.

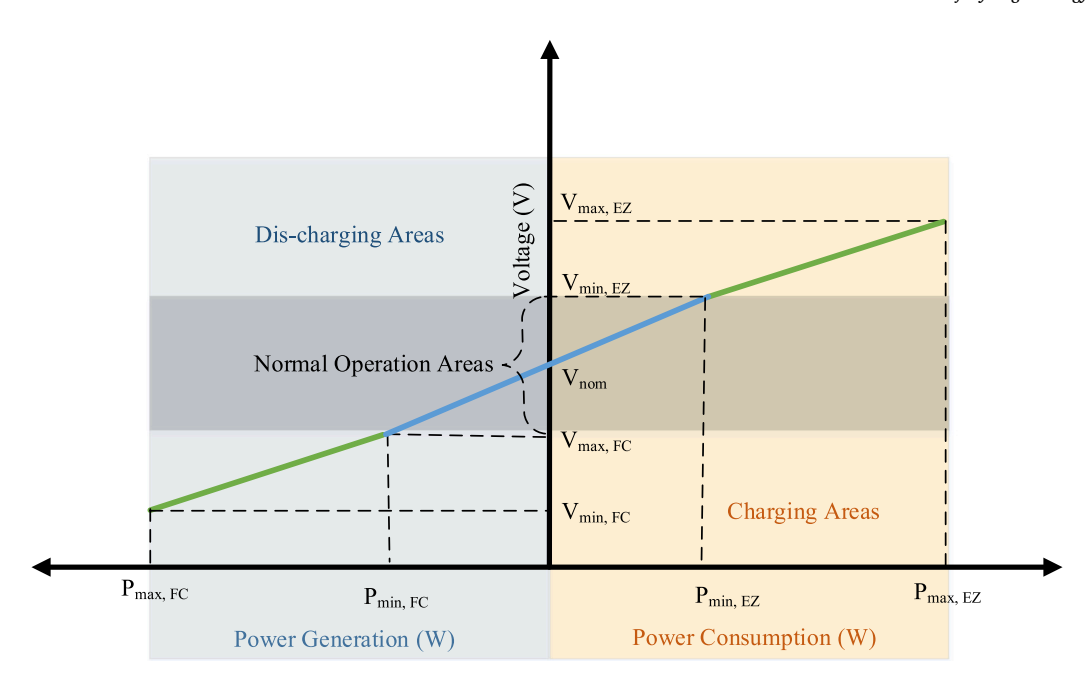


Fig. 3. DC link voltage-based operational principles.

# 3.3. Stability analysis

The droop control-based voltage regulation assumes small-signal perturbations around the nominal operating voltage. The following assumptions are explicitly stated: (1) Small deviations around the nominal operating voltage  $V_{ref}$ ; (2) Linear approximation of system dynamics near equilibrium points; (3) Component behaviours modelled via linearised second-order dynamics derived from empirical data; and (4) Linear response within operational bandwidth for electrolysers, fuel cells, and battery storage.

Droop control strategy defines the power response to voltage deviations as:

$$P(t) = K_v \left( V_{ref} - V_{dc}(t) \right) \tag{17}$$

Linearising around equilibrium points  $(P_0, V_0 = V_{ref})$ :

$$P(t) = P_0 + \Delta P(t), \quad V_{dc}(t) = V_0 + \Delta V(t)$$
 (18)

Thus, for small deviations:

$$\Delta P(t) = -K_{\nu} \Delta V(t) \tag{19}$$

The DC-link voltage dynamics are governed by:

$$C_{dc}\frac{dV_{DC}(t)}{dt} = P_{gen}(t) - P_{load}(t)$$
 (20)

Expressed in small-signal terms:

$$C_{dc}\frac{d(\Delta V(t))}{dt} = \Delta P_{gen}(t) - \Delta P_{load}(t) \tag{21} \label{eq:21}$$

Considering droop control responses for fuel cell (generation), electrolyser (load), and battery (bi-directional):

$$\Delta P_{FC}(t) = -K_{fc} \Delta V(t), \tag{22}$$

$$\Delta P_{EZ}(t) = -K_{ez}\Delta V(t), \tag{23}$$

$$\Delta P_{Bat}(t) = -K_b \Delta V(t) \tag{24}$$

Hence, the combined small-signal power deviation is:

$$\Delta P_{total}(t) = -(K_{fc} + K_b + K_{ez})\Delta V(t)$$
 (25)

This gives the simplified voltage dynamic equation:

$$C_{dc}\frac{d(\Delta V(t))}{dt} = -(K_{fc} + K_b + K_{ez})\Delta V(t)$$
 (26)

Rearranging:

$$\frac{d(\Delta V(t))}{dt} + \frac{(K_{fc} + K_b + K_{ez})}{C_{dc}} \Delta V(t) = 0$$
 (27)

This first-order differential equation takes the form:

$$\frac{d(\Delta V(t))}{dt} + a\Delta V(t) = 0,$$

$$(K_{+} + K_{+} + K_{-})$$
(28)

where 
$$a = \frac{(K_{fc} + K_b + K_{ez})}{C_{dc}} > 0$$
 (29)

The general solution is:

$$\Delta V(t) = \Delta V(0)e^{-at} \tag{30}$$

Since a>0, voltage deviations decay exponentially, indicating asymptotic stability.

# 4. Experimental validation

The effectiveness of the proposed DCVC framework in managing an islanded DC microgrid is demonstrated in this section. The dynamic controllers have been applied to a fuel cell emulator, an electrolyser emulator, and battery banks, enabling flexible microgrid operation. The battery control system plays a central role in ensuring reliable and secure microgrid operation. The solar, wind and wave generators are emulated using 1 kW Kepco four-quadrant (bipolar) power supply. The fuel cells are also emulated using the 1 kW power supply while the electrolyser is emulated using a 1.8 kW ITECH programmable AC/DC electronic load. All the renewable energy generation data presented here are general indicative patterns and can be easily adapted for specific datasets. The entire code is implemented in the JavaScript environment using the Node-RED platform. Communication of electrolyser and load simulator data occurs through Ethernet and CAN lines using the Node-RED platform. The coding is executed on a small-scale computer — an 8 GB Raspberry Pi 5. For visualisation of outcomes, the open-source and powerful visualisation software Grafana is employed. The industry standard experiment for the hydrogen microgrid is demonstrated in Fig. 5. Both the software and hardware components used in this experiment are cost-effective compared to commercial alternatives. The utilisation of an open-source platform avoids the expensive subscription costs associated with commercial software, such as LabView.

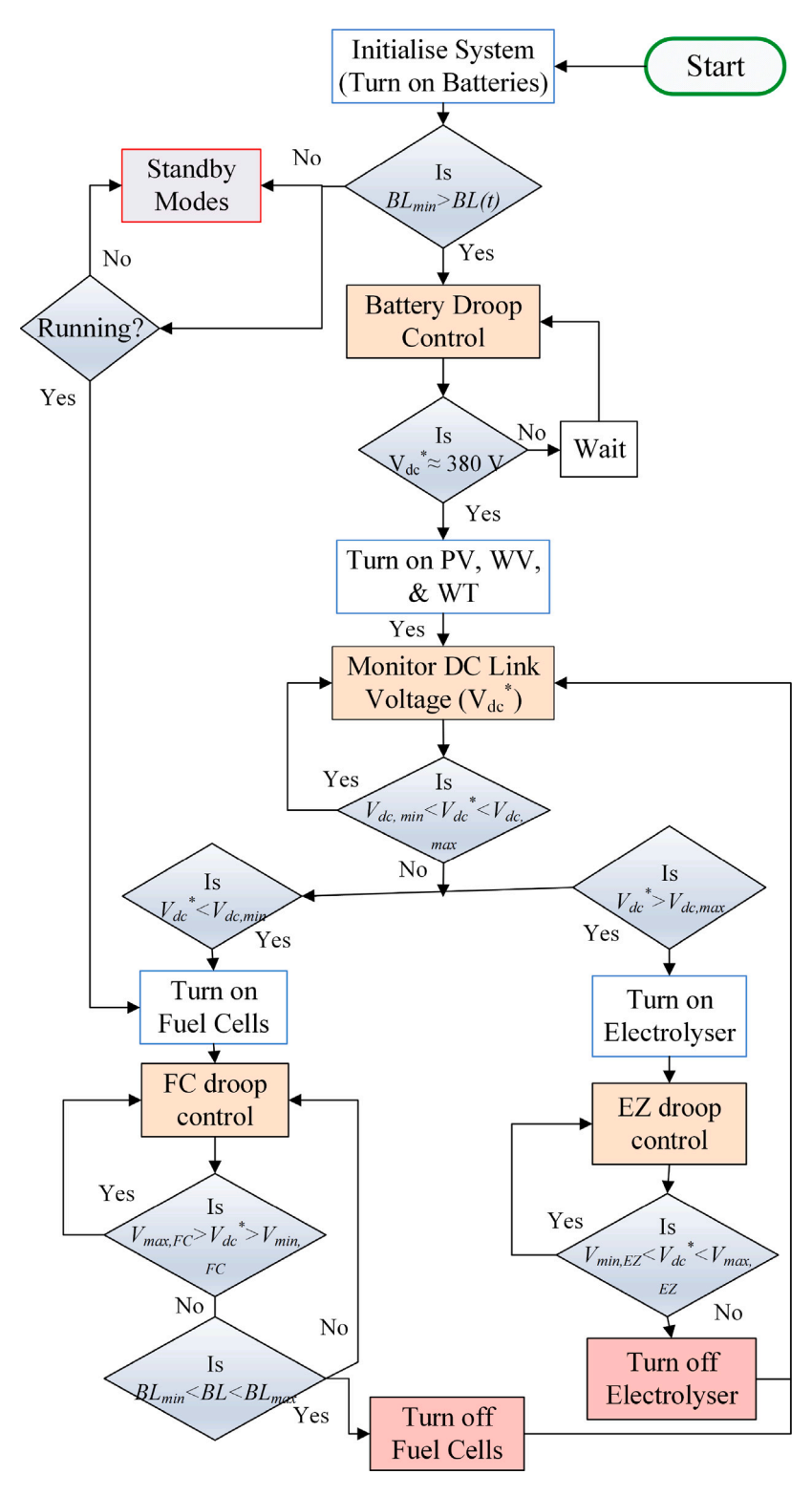


Fig. 4. The flowchart of the autonomous algorithm.

In the following sections, various case studies to illustrate the effectiveness of the proposed control framework are conducted. Each case study aims to showcase specific aspects of the microgrid's performance under various scenarios.

# 4.1. Case 1: Operation of the electrolyser

This case study explores the operation of the electrolyser, em-

phasising its role in stabilising the DC link voltage within specified limits for the reliable operation of the microgrid. The experiment was conducted under intermittent renewable power input, resulting in natural fluctuations in the DC link voltage. These fluctuations caused the electrolyser to automatically activate in response to overvoltage conditions (> 385 V) and deactivate when voltage dropped below 378 V. Data was collected at a sampling frequency of 0.5 Hz using the Raspberry Pi controller. The DC voltage and electrolyser power data



Fig. 5. The industry standard experimental set-up at Griffith University.

were analysed using time-domain techniques to extract transient characteristics, including rise time, settling time, overshoot, and oscillation frequency. Fig. 6 presents the electrolyser's operation, highlighting the dynamic production of hydrogen. The electrolyser adjusts its hydrogen production in response to the DC link voltage: increasing production when the voltage is high (approaching 390 V) and reducing production when the voltage is lower (near 380 V).

The electrolyser operates automatically based on the DC link voltage levels. It starts functioning when the voltage exceeds 385 V, as observed at 18:05:20, and shuts down when the voltage drops below 378 V, as seen at the end of 18:08:40. This automatic response helps maintain voltage stability within the microgrid.

The data analysis of the electrolyser's first transient response reveals several key characteristics indicative of its power consumption behaviour and dynamic performance. The peak value of the power consumption reaches 1104 watts, significantly higher than the steady state value of 769 watts, suggesting a substantial initial power surge. The system's rise time of 1.113 s indicates a relatively swift response to the input signal, achieving near-peak power consumption quickly. However, the settling time of 53.6347 s implies a prolonged period before the power consumption stabilises around the steady state value, reflecting the electrolyser's need to overcome initial fluctuations. The overshoot of 43.5631% is notable, indicating that the power consumption exceeds the steady state by a considerable margin during the initial transient phase, which could be attributed to the inertia and internal resistance of the electrolyser. The frequency of oscillation at 0.125 Hz denotes a slow oscillatory behaviour, which suggests that the system experiences periodic fluctuations in power consumption before reaching equilibrium. These transient characteristics highlight the electrolyser's dynamic response under operational conditions, emphasising the importance of optimising control strategies to mitigate overshoot and reduce settling time, thereby enhancing overall system efficiency and stability.

Given the transient behaviour, the electrolyser is modelled as a second-order dynamic system whose response to voltage variations is represented through an experimentally derived transfer function:

$$G_{EZ}(s) = \frac{K_{EZ}}{\tau_{EZ}^2 s^2 + 2\zeta_{EZ}\tau_{EZ}s + 1}$$
 (31)

where the parameters are explicitly identified through experiments:

• Steady-state gain:  $K_{EZ} = 769 \,\text{W/V}$ 

• Time constant:  $\tau_{EZ} = 3.1 \,\mathrm{s}$ 

• Damping ratio:  $\zeta_{EZ} = 0.228$ 

These parameters were empirically derived from the electrolyser's transient response to step-changes in the DC-link voltage. The physical

interpretation of this second-order behaviour can include two dominant dynamics: electrochemical reaction kinetics at the electrodes and thermal/mass-transport phenomena within the electrolyser stack.

The electrolyser's dynamic parameters were identified using a leastsquares fitting approach applied to measured transient experimental data, fitting to the canonical second-order step-response equation:

$$y(t) = y_{\text{final}} \left[ 1 - \frac{e^{-\zeta \omega_n t}}{\sqrt{1 - \zeta^2}} \sin\left(\omega_n \sqrt{1 - \zeta^2} t + \phi\right) \right]$$
 (32)

where the natural frequency is  $\omega_n = \frac{1}{\tau_{EZ}}$  and the phase shift  $\phi$  is obtained from experimental data. A comparison between the dynamic model response and the experimental response is presented in Fig. 7 to validate the model.

At 18:06:50 in Fig. 6(a), the transient behaviour of the electrolyser is not fully reflected except for a small spike. This is because the DC link voltage reaches its maximum value of 390 V, where the transient effect of the electrolyser operation is minimal. At this voltage level, the electrolyser operates smoothly with reduced transient fluctuations, ensuring stable DC link voltage.

The electrolyser's transient behaviour also influences the flexible battery power supply. The battery system adjusts accordingly to support the microgrid, ensuring a stable and reliable power supply, shown in Fig. 6(c). The power generation pattern, including wave generator data, is indicative of typical operation shown in Figs. 6(b), 6(d), and 6(f). In practice, wave power generation is more stable and predictable compared to wind and solar power, which means variations in power generation patterns do not significantly impact the overall microgrid operation.

In summary, the electrolyser effectively stabilises the DC link voltage by dynamically adjusting hydrogen production in response to voltage changes. Its operation ensures the microgrid remains within safe and reliable voltage limits. The detailed transient response analysis demonstrates the electrolyser's quick reaction to voltage changes and minimal transient effects at high voltage levels. Additionally, the integration of the electrolyser with the battery system and other renewable sources highlights the microgrid's capability to maintain stability and efficiency in varying operational conditions.

# 4.2. Case 2: Operation of fuel cells

This section focuses on the autonomous operation of fuel cells, aiming to maintain stable DC link voltage within defined limits to ensure the reliable and secure operation of the microgrid. Under normal conditions, the fuel cells remain inactive. However, they automatically activate when power generation significantly falls below demand, ensuring economical and reliable system operation. To analyse the fuel

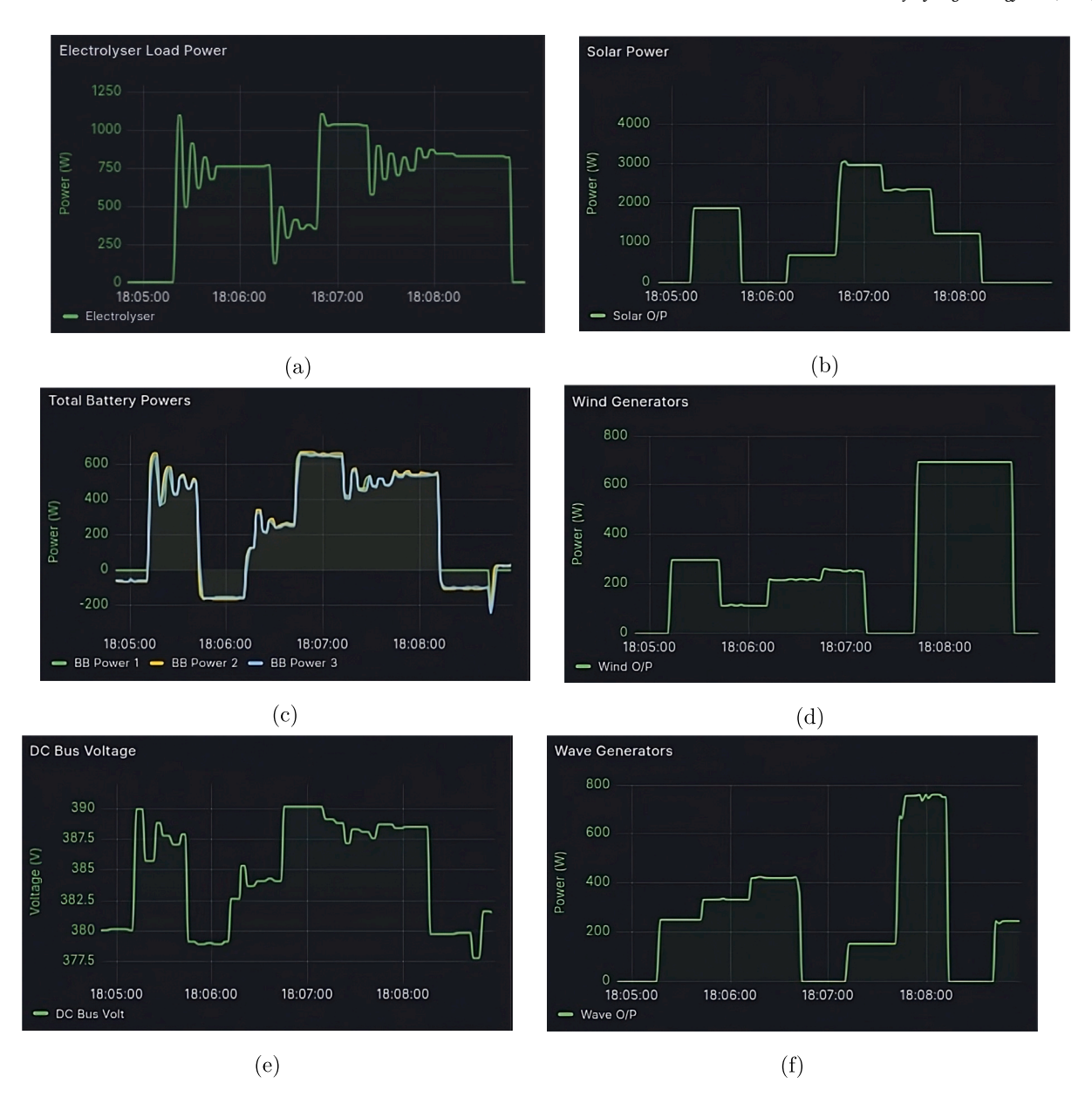


Fig. 6. Electrolyser's operation based on DC link voltage: (a) electrolyser, (b) solar generator, (c) battery banks, (d) wind generator, (e) DC link and (e) wave generator.

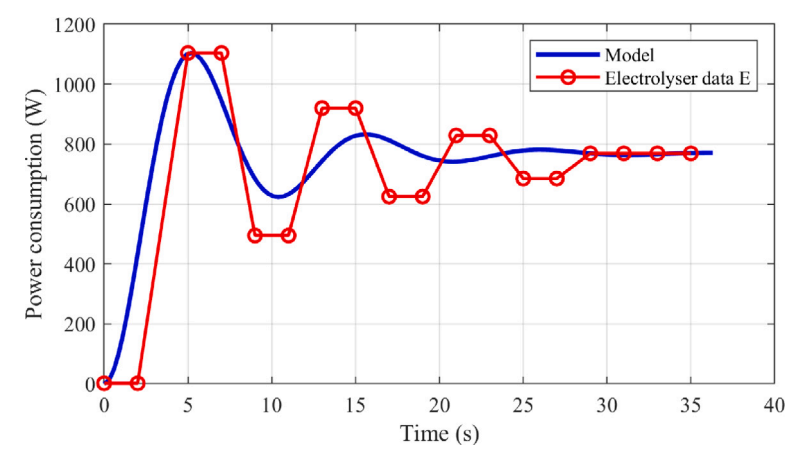


Fig. 7. Dynamic modelling response of electrolyser vs practical data response.



Fig. 8. Fuel cell's operation based on DC link voltage: (a) fuel cells, (b) loads, (c) battery banks, (d) wind generator, (e) DC link and (f) wave generator.

cell's transient response, a baseline load of 3.5/2.5 kW was applied with no solar generation, ensuring the fuel cell's autonomous role could be clearly observed. The system's data were recorded every 2 s and stored in an InfluxDB database running on the Raspberry Pi. The data was exported in Excel format and analysed using MATLAB to calculate key transient response parameters, including rise time, overshoot, and settling time.

Fuel cells activate when they detect a lower DC link voltage, such as 375 V, indicating insufficient power generation compared to demand. Fig. 8(a) illustrates the operation of the fuel cells, showing transient power delivery in response to load changes. The fuel cells dynamically adjust their power output to meet the changing power demands. During poor power generation, the fuel cells run at full capacity, resulting in a low DC link voltage, such as 370 V, as depicted in Fig. 8(e).

The data analysis of the fuel cell's transient response, as illustrated in Fig. 8, reveals several key characteristics indicative of its power generation behaviour and dynamic performance. The peak value of the power generation reaches 660.00 watts, which is significantly higher than the steady state value of 411.50 watts, indicating a substantial initial surge in power output. The system's rise time of 2.00 s suggests a

relatively quick response to the input signal, reaching near-peak power generation swiftly. However, the settling time of 75.00 s indicates a prolonged period before the power output stabilises around the steady state value, reflecting the fuel cell's challenge in overcoming initial fluctuations. The overshoot of 60.39% is particularly notable, showing that the power generation exceeds the steady state by a considerable margin during the initial transient phase, which could be attributed to the inertia and internal resistance of the fuel cell. The frequency of oscillation at 0.091 Hz denotes a slow oscillatory behaviour, suggesting that the system experiences periodic fluctuations in power generation before reaching equilibrium. These transient characteristics underscore the dynamic response of the fuel cell under varying operational conditions, highlighting the need for optimising control strategies to mitigate overshoot and reduce settling time, thereby improving overall system efficiency and stability.

The transfer function representing the dynamic response of the fuel cell system, including the droop controller can be represented as

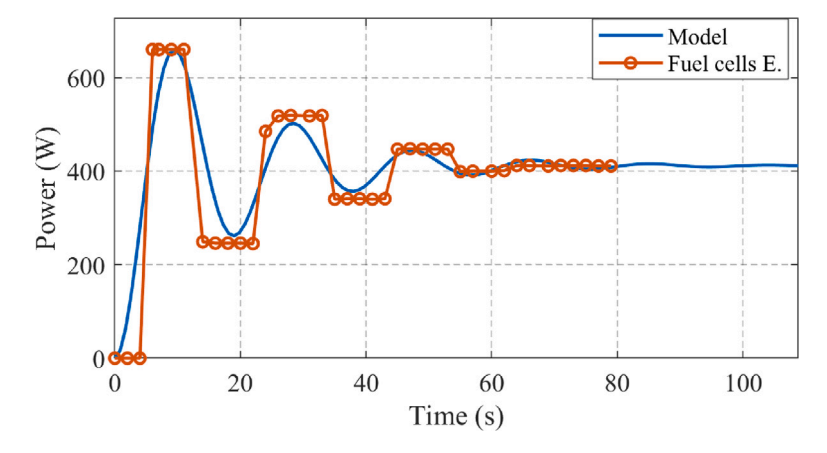


Fig. 9. Dynamic modelling response of fuel cells vs practical data response.

follows:

$$G_{FC}(s) = \frac{K_{FC} \,\omega_{n,FC}^2}{s^2 + 2\zeta_{FC} \,\omega_{n,FC} s + \omega_{n,FC}^2} \tag{33}$$

where the experimentally identified parameters are:

• Steady-state gain:  $K_{FC} = 411 \,\text{W/V}$ 

• Natural frequency:  $\omega_{n,FC} = 0.3365 \, \text{rad/s}$ 

• Damping ratio:  $\zeta_{FC} = 0.1585$ 

This transfer function model characterises the transient behaviour of the fuel cell system when it responds to load changes, including the observed overshoot, rise time, and oscillatory behaviour. For validation purposes, Fig. 9 shows the step response of the dynamic model as compared to the response of the fuel cell emulator (E.).

The fuel cell dynamics can exhibit second-order behaviour due to inherent electrochemical processes, catalyst reaction kinetics, thermal management, and water transport phenomena inside the fuel cell stack. Similar to the electrolyser, the parameters were explicitly determined by fitting experimental transient step-response data to the standard second-order dynamic response formulation.

This experiment was conducted without running the solar power generator to appropriately evaluate the operation of the fuel cells. The absence of solar power generation allows for a clearer observation of the fuel cells' autonomous response to varying power demands and their impact on maintaining a stable DC link voltage.

In summary, the autonomous operation of fuel cells plays a crucial role in stabilising the DC link voltage within a microgrid. By dynamically adjusting their power output in response to changes in power demand, the fuel cells ensure reliable and economical operation. The detailed analysis of the transient response parameters demonstrates the fuel cells' effectiveness in quickly stabilising the DC link voltage, even in the absence of solar power generation. This capability is essential for maintaining the overall stability and efficiency of the microgrid.

# 4.3. Case 3: Autonomous operation of the hydrogen microgrid

In this case study, the focus is on the autonomous operation of the hydrogen microgrid, where the dynamics of hydrogen fuel cells and electrolysers play a pivotal role in maintaining stability and reliability. This experiment was conducted under a dynamic load profile ranging from approximately 0 kW to 6 kW, with simulated PV generation input held constant during the test window. The system operated autonomously using voltage-based triggering for both electrolyser and fuel cell activation. Fig. 10 provides a comprehensive illustration of this autonomous operation.

Initially, when renewable energy generation surpasses load demands, resulting in a higher DC link voltage at time 21:20:40, the

system autonomously triggers the activation of the electrolyser shown in Fig. 10(d). The electrolyser then starts with a transient phenomenon to produce hydrogen, guided by the voltage controller. This proactive response manages the excess renewable power and facilitates the storage of hydrogen for future use.

As power demand gradually increases (Fig. 10(b)) while renewable generation remains constant (Fig. 10(f)), the DC-link voltage drops below 375 V (Fig. 10(d)). In response, the fuel cell automatically activates to stabilise the voltage, as illustrated in Fig. 10(c). The fuel cell initiates power production in accordance with the voltage control strategy outlined in Section 4. Fig. 10(c) showcases how fuel cells dynamically adjust their power output to meet evolving power demands, ensuring a reliable and stable power supply.

It is worth noting that the electrolyser and fuel cells will not run simultaneously due to different voltage settings that indicate the status of power generation and power demand, which is captured in Figs. 10(a) and 10(c). This separation ensures efficient management of the microgrid's resources.

The intricate relationship between power generation and demand is visualised by monitoring the DC link voltage, which provides a comprehensive overview of the system's performance. The autonomous operation of the hydrogen microgrid, supported by the coordinated interplay of the electrolyser and fuel cells, exemplifies an adaptive and responsive power control system.

In summary, the hydrogen microgrid effectively balances the fluctuating nature of renewable energy sources with varying power demands, contributing to the overall resilience and sustainability of the microgrid. This adaptive and responsive power control system ensures that the microgrid can maintain stability and reliability, even as power demands and renewable energy generation fluctuate. The coordinated operation of the electrolyser and fuel cells provides a robust solution for managing power within the microgrid, enhancing its performance and sustainability.

# 4.4. Case 4: Comparison of electrolyser operation

In this experiment, a comparison of the electrolyser's dynamic behaviour was carried out under two operating modes: manual control (without droop) and autonomous control (with droop). The manual case was implemented by adjusting the electrolyser's power demand manually, while the droop-controlled case followed the automated strategy described in Section 3. In both scenarios, the system started at 0 W and underwent a step increase and decrease in power demand. Experimental data were logged in real-time using InfluxDB, exported in .xls format, and processed in MATLAB for side-by-side analysis. From Fig. 11, it can be observed that during the initial 0 to 15 samples, both systems — regardless of whether the droop controller is enabled — begin with a power demand of approximately 0 watts. During

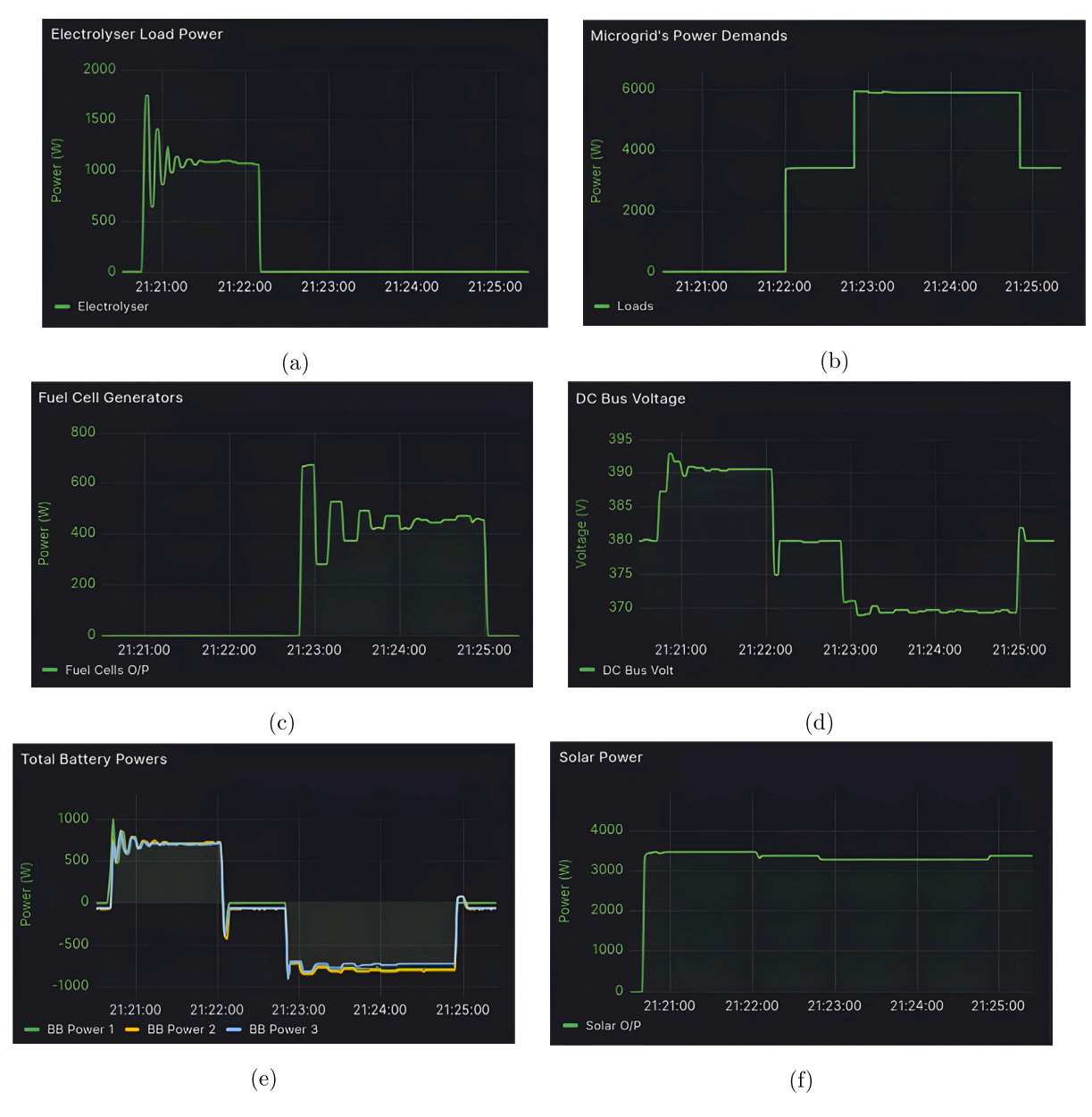


Fig. 10. Autonomous operation: (a) electrolysers, (b) loads, (c) fuel cells, (d) DC link, (e) battery banks, and (f) solar generation.

this period, their behaviours are synchronised, with both maintaining identical power levels. In the mid-phase of the graph, covering from 15 to 55 samples, a clear difference emerges between the two systems. The system without the droop controller exhibits a step response, where the power demand abruptly increases to around 750 watts. In contrast, the system with the droop controller first shows an overshoot, with power demand spiking above 1000 watts before settling around 750 watts. This system also displays noticeable fluctuations during this period.

Oscillations in the droop-controlled case arise from real-time voltage-feedback-driven corrections, which may overreact to transient events. In contrast, manual control operates in an open-loop fashion, applying fixed setpoints without reacting to voltage deviations, resulting in more stable transitions.

As the power demand of the electrolyser is influenced by the network power demand from 40 to 60 samples, the system without the droop controller manually decreases its power demand to about 350 watts and maintains this level consistently. The droop-controlled system also reduces its power demand to 350 watts, but with significant oscillations before it begins to stabilise around the same power level,

although with persistent minor fluctuations. In the final phase of the electrolyser operation, from 90 to 120 samples, both systems show a synchronised behaviour similar to the initial phase. The power demand gradually decreases to around 0 watts for both systems.

In summary, the comparison between manual and droop-controlled electrolyser operation highlights key trade-offs in transient performance, responsiveness, and operational efficiency. The droop-controlled system demonstrated a dynamic response during power transitions, including initial overshoot and oscillations, while the manually controlled system exhibited a smoother response, requiring continuous human intervention to track load changes.

In this experiment, although manual operation reduces voltage fluctuations, it is challenging for real-world deployment due to its dependence on constant operator input. Additionally, staffing a full-time operator in a remote microgrid can incur a recurring cost of approximately AUD \$80,000 per year, which is not justified when autonomous control can be achieved using a low-cost, open-source embedded controller. Furthermore, delayed or imprecise manual responses can lead to hydrogen overproduction, underutilisation of renewable inputs, or

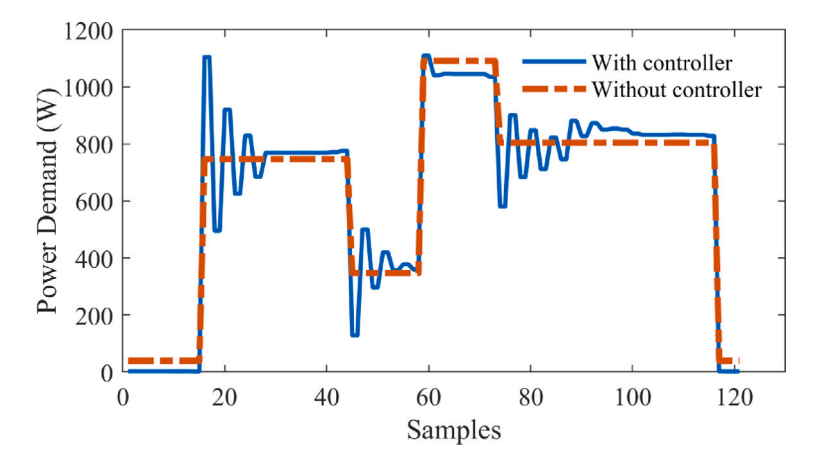


Fig. 11. Comparison of electrolyser operation with and without droop controller. Experimental data are collected using xls format from Grafana wavepage, which has been plotted on Matlab for side-by-side comparison.

excessive component cycling — all of which increase maintenance costs and reduce system lifespan.

To quantify the economic implications at scale, consider a 100 MW electrolyser operating without real-time coordination. A modest 2% daily inefficiency from delayed adjustments or curtailments results in 2 MWh/day of hydrogen energy loss. Assuming 50 kWh/kg production efficiency and a hydrogen price of AUD \$6/kg, this equates to 40 kg/day, or roughly AUD \$240/day, amounting to nearly AUD \$87,600 per year in unrealised value — a significant loss in long-term islanded or grid-constrained projects.

By contrast, the droop-controlled approach provides fully autonomous operation, faster transient tracking, and adaptability to renewable fluctuations. While it introduces minor oscillations, these can be mitigated through filter integration — aspects that will be explored in future research. The benefits of automation, cost reduction, and dynamic performance make droop-based control especially suited for systems with high renewable penetration, limited communication infrastructure, or islanded microgrids. For applications prioritising minimal fluctuations — such as preserving electrolyser durability — a hybrid strategy combining predictive smoothing with adaptive droop control may provide the most effective balance between performance and protection.

# 4.5. Case 5: Comparison of battery controller application

In this case, the battery controller's impact on voltage regulation was assessed by toggling its activation status under variable loading conditions. The experiment consisted of no-load and load intervals introduced at approximately 10:40 and 11:05, with the controller being alternately enabled and disabled. Voltage response and battery power were recorded using a 0.5 Hz sampling rate. The aim was to quantify the controller's influence on voltage dip suppression and steady-state regulation across different system states.

The DC link voltage in the microgrid, comparing its performance with and without the application of a controller, is demonstrated in Fig. 12(a). It represents the voltage fluctuations over time, giving insight into the system's behaviour under both conditions. The comparison between the two phases — before and after the controller is activated — highlights the controller's vital role in enhancing system performance. Before its activation, the voltage remains at a lower value of around 374V. After the controller is engaged, the system reaches a higher voltage, demonstrating the controller's effectiveness in regulating and maintaining the desired voltage level in the microgrid. This illustrates the importance of active control mechanisms in ensuring the stable and reliable operation of such systems.

To further extend the comparison, Fig. 12(b) illustrates the behaviour of the DC link voltage in the microgrid under different loading

conditions, highlighting the performance with and without a controller. Two distinct regions are marked as "No load" at around 10:40 and 11:05, where the voltage stabilises near 380 V without any load. In the central portion, labelled as the "Load" condition, the voltage initially drops to around 375 V when a load is applied.

When the system operates without a controller, the initial voltage under the no-load condition is approximately 372.5 V. If the controller is activated, then the voltage reaches 380 V. In this condition, the load is introduced, and there is a noticeable dip in voltage, marking around 376 V. In contrast, when the controller is deactivated for a short while, the voltage dip below 370 V. The bus voltage stabilises at around 375 V when the controller is reactivated under load, demonstrating the controller's ability to regulate the bus voltage more effectively, even under varying load conditions. The turning on and off of the load is demonstrated in Fig. 12(c) and the corresponding battery power drawn by the network is shown in Fig. 12(d).

# 4.6. Discussion

The observed overshoots of approximately 43% in the electrolyser emulator and 60% in the fuel cell emulator during transient events are primarily attributed to abrupt step changes in the load demand. These transitions challenge the response time of the power electronic converters and the intrinsic dynamic delays of hydrogen-based devices. While the system successfully stabilised within acceptable settling times, such high overshoots — if occurring frequently — can exert considerable stress on critical components such as DC/DC converters, valves, and control circuitry. This repeated stress may accelerate wear, thermal degradation, and reduce the operational lifespan of the system, particularly under harsh or isolated conditions where component replacement is difficult. To address this, integrating predictive control elements such as model-based damping filters or feedforward compensators could help suppress the initial transient magnitude. The overshoots can also be minimised by implementing low-pass filters or derivative-based filtering techniques in the control loop, which smooth sudden reference changes and mitigate the impact of sharp load transitions. These advanced control strategies will be systematically explored and tested in future work to further enhance the system's stability, responsiveness, and reliability under diverse dynamic operating conditions.

While the current control strategy primarily relies on voltage deviation as a key feedback signal for coordinating multiple sources, this approach can be further enhanced by integrating additional system state variables into the decision-making process. In future developments, incorporating multi-variable indicators such as battery state of charge, hydrogen storage tank pressure, fuel cell/electrolyser temperature, and hydrogen purity levels could enable a more context-aware and adaptive control framework. These parameters would allow for more

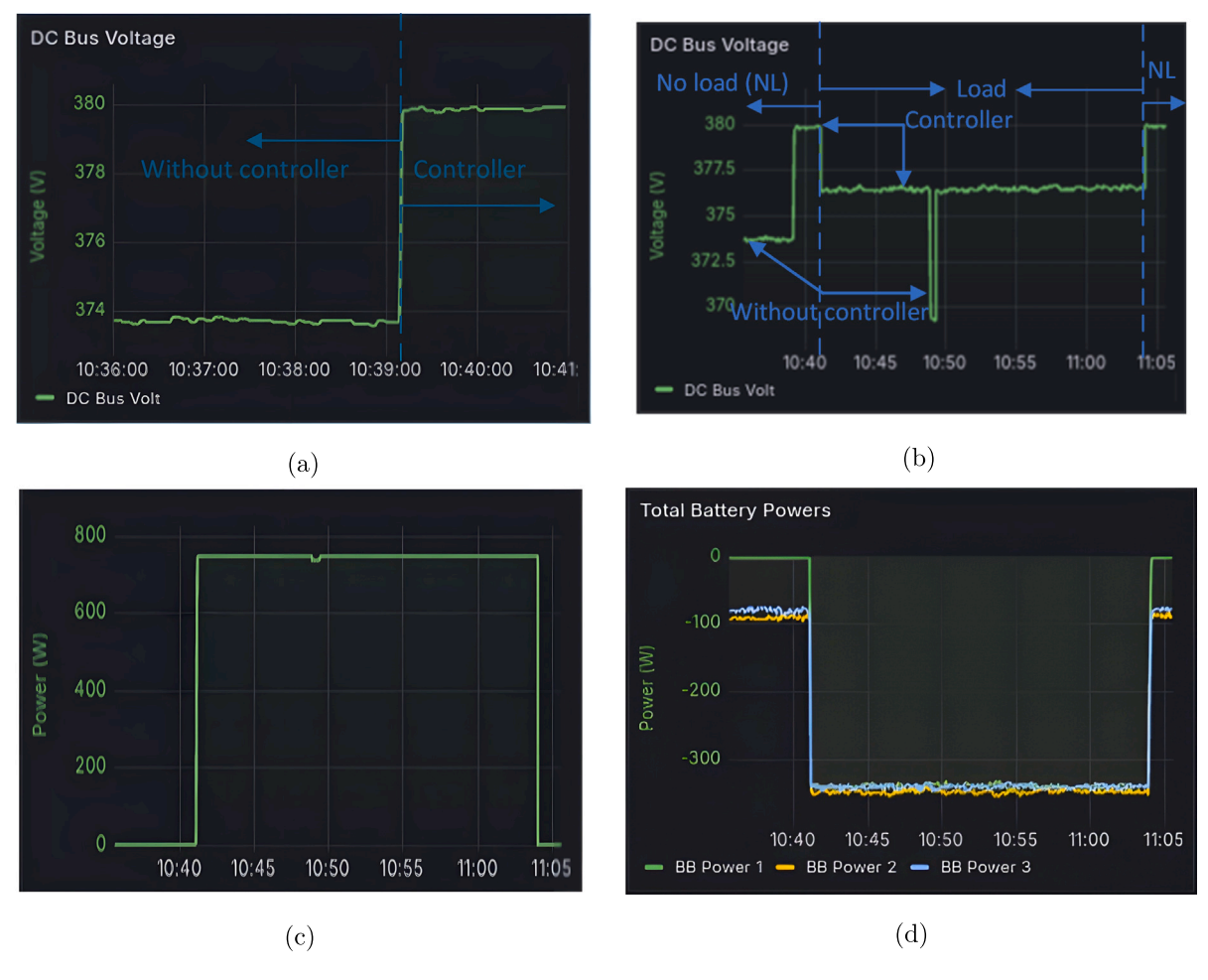


Fig. 12. Comparative study with and without the battery controller (a) DC bus voltage, (b) DC bus voltage extended, (c) Load demands and (d) Battery powers.

intelligent prioritisation of energy sources based on resource availability, component health, and operational constraints, thereby improving overall system resilience, efficiency, and lifetime performance.

The proposed control improves the system's operational efficiency by minimising unnecessary hydrogen cycling and better aligning power supply with demand. Compared to uncoordinated operation, this reduces energy losses and enhances the lifespan of electrolysers and fuel cells, contributing to lower operational costs. While detailed economic analysis is beyond the current scope, future work will focus on modelling cost savings and assessing the overall economic viability of the system.

# 5. Conclusions

This study proposed and experimentally validated a novel DC-link Voltage Control (DCVC) framework for islanded hydrogen DC microgrids that ensures stable, autonomous, and efficient operation under varying renewable generation and load conditions. The framework is based on adaptive droop control principles and includes dynamic voltage regulation mechanisms for fuel cells, electrolysers, and battery systems. In addition to experimental validation, a small-signal model of the proposed DC-link control framework was developed for fuel cell, electrolyser, and battery systems. The resulting voltage dynamic equation confirms that the system exhibits exponentially decaying voltage deviations, ensuring stable operation even under fluctuating power conditions.

Comprehensive hardware-in-the-loop testing on an industry-standard hydrogen DC microgrid platform demonstrated the efficacy of the proposed approach across five operational case studies. Key findings include:

- Electrolyser operation: The voltage-responsive hydrogen production control maintained DC-link voltage stability with a 43.56% overshoot and 53.63s settling time, highlighting the need for tailored transient mitigation strategies.
- Fuel cell performance: The controller dynamically regulated hydrogen injection in response to voltage under-shoots, with a rapid 2s rise time and 75s settling time, enabling reliable support during power shortages.
- Battery control: Battery droop control minimised voltage oscillations during load fluctuations, stabilising the DC bus around 380 V and significantly enhancing microgrid reliability under dynamic conditions.
- Coordinated operation: The autonomous algorithm effectively balanced the interactions among all distributed resources, enabling intelligent source prioritisation and hydrogen-battery synergy under both high and low generation scenarios.

Compared to fixed-priority or rule-based systems, the adaptive droop approach demonstrated superior flexibility, scalability, and control granularity — especially under experimental disturbances and varying load/generation profiles. In practice, it reduces manual tuning and adapts autonomously to system changes.

Moreover, by leveraging cost-effective hardware (Raspberry Pi, Node-RED, and Grafana) and experimentally derived transfer functions, this work bridges the gap between simulation-heavy studies and real-world deployment. The resulting control architecture is fully replicable, low-cost, and suitable for decentralised energy systems in remote, offshore, or aquaculture-based applications, where commercial SCADA systems or centralised dispatch are expensive.

While Model Predictive Control (MPC) remains a powerful technique for constrained optimisation and multi-objective control, its structure, complexity, and centralisation requirements differ significantly from the real-time, decentralised droop-based framework presented in this study. As such, a direct performance comparison with MPC is beyond the scope of this work and would not constitute a fair or equivalent evaluation.

Future work will focus on extending the controller to a nonlinear or multi-input adaptive form (e.g., voltage + BL(t) + hydrogen level), improving real-time gain scheduling algorithms, and enabling inter-microgrid communication and coordination in larger networks.

#### Declaration of competing interest

The authors declare that they have no known competing financial interests or personal relationships that could have appeared to influence the work reported in this paper.

# Acknowledgment

The authors gratefully acknowledge the financial support provided by the Blue Economy Cooperative Research Centre, which is established and supported under the Australian Government's CRC Program (grant number CRC-20180101). The CRC Program aims to foster industry-led collaborations between various stakeholders, including industry partners, researchers, and the community. The assistance of D. Wilding in developing the battery management system and building the microgrid is gratefully acknowledged.

#### References

- [1] Hosseini SM, Carli R, Dotoli M. Robust optimal energy management of a residential microgrid under uncertainties on demand and renewable power generation. IEEE Trans Autom Sci Eng 2020;18(2):618–37.
- [2] Hossain MA, Pota HR, Hossain MJ, Blaabjerg F. Evolution of microgrids with converter-interfaced generations: Challenges and opportunities. Int J Electr Power Energy Syst 2019;109:160–86.
- [3] Dragičević T, Lu X, Vasquez JC, Guerrero JM. DC microgrids—Part II: A review of power architectures, applications, and standardization issues. IEEE Trans Power Electron 2015;31(5):3528–49.
- [4] Khan MA, Onwuemezie L, Darabkhani HG. Low-carbon fuelled MGT-chp system coupled with PEM electrolyser and fuel cell units: A fuel flexibility and performance study. Int J Hydrog Energy 2024;58:1277–83.
- [5] Abdelghany MB, Mariani V, Liuzza D, Natale OR, Glielmo L. A unified control platform and architecture for the integration of wind-hydrogen systems into the grid. IEEE Trans Autom Sci Eng 2023.
- [6] Yıldız S, Gunduz H, Yildirim B, Özdemir MT. An islanded microgrid energy system with an innovative frequency controller integrating hydrogen-fuel cell. Fuel 2022;326:125005.
- [7] Erdemir D, Dincer I. Development of renewable energy based green hydrogen and oxygen production and electricity generation systems for sustainable aquaculture. J Clean Prod 2024;434:140081.

- [8] Oyewole OL, Nwulu NI, Okampo EJ. Optimal design of hydrogen-based storage with a hybrid renewable energy system considering economic and environmental uncertainties. Energy Convers Manage 2024;300:117991.
- [9] Coppitters D, Verleysen K, De Paepe W, Contino F. How can renewable hydrogen compete with diesel in public transport? robust design optimization of a hydrogen refueling station under techno-economic and environmental uncertainty. Appl Energy 2022;312:118694.
- [10] Hou R, Maleki A, Li P. Design optimization and optimal power management of standalone solar-hydrogen system using a new metaheuristic algorithm. J Energy Storage 2022:55:105521.
- [11] Abdelghany MB, Mariani V, Liuzza D, Glielmo L. Hierarchical model predictive control for islanded and grid-connected microgrids with wind generation and hydrogen energy storage systems. Int J Hydrog Energy 2024;51:595–610.
- [12] Abdelghany MB, Al-Durra A, Zeineldin H, Hu J. Integration of cascaded coordinated rolling horizon control for output power smoothing in islanded wind–solar microgrid with multiple hydrogen storage tanks. Energy 2024;291:130442.
- [13] Martínez L, Fernández D, Mantz R. Passivity-based control for an isolated DC microgrid with hydrogen energy storage system. Int J Hydrog Energy 2024.
- [14] Brka A, Kothapalli G, Al-Abdeli YM. Predictive power management strategies for stand-alone hydrogen systems: Lab-scale validation. Int J Hydrog Energy 2015;40(32):9907–16.
- [15] Brka A, Al-Abdeli YM, Kothapalli G. Predictive power management strategies for stand-alone hydrogen systems: Operational impact. Int J Hydrog Energy 2016;41(16):6685–98.
- [16] Martínez L, Fernández D, Mantz R. Two layer control strategy of an island DC microgrid with hydrogen storage system. Int J Hydrog Energy 2024;50:365–78.
- [17] Zhu Z, Liu X, Kong X, Ma L, Lee KY, Xu Y. PV/Hydrogen DC microgrid control using distributed economic model predictive control. Renew Energy 2024;222:119871.
- [18] Kilic H. Improving the performance of microgrid-based power-to-x systems through optimization of renewable hydrogen generation. Int J Hydrog Energy 2024.
- [19] Khani H, El-Taweel NA, Farag HEZ. Supervisory scheduling of storage-based hydrogen fueling stations for transportation sector and distributed operating reserve in electricity markets. IEEE Trans Ind Inform 2019;16(3):1529–38.
- [20] Abomazid AM, El-Taweel NA, Farag HE. Optimal energy management of hydrogen energy facility using integrated battery energy storage and solar photovoltaic systems. IEEE Trans Sustain Energy 2022;13(3):1457–68.
- [21] Yang Y, Jia Q-S, Guan X, Zhang X, Qiu Z, Deconinck G. Decentralized EV-based charging optimization with building integrated wind energy. IEEE Trans Autom Sci Eng 2018;16(3):1002–17.
- [22] Bexell M, Jönsson K. Responsibility and the united nations' sustainable development goals. In: Forum for development studies. 44, (1):Taylor & Francis; 2017, p. 13–29.
- [23] Sundararajan SCM, Shankar YB, Selvam SP, Manogaran N, Seerangan K, Natesan D, Selvarajan S. IoT-based prediction model for aquaponic fish pond water quality using multiscale feature fusion with convolutional autoencoder and GRU networks. Sci Rep 2025;15(1):1925.
- [24] Hossain MA, Pota HR, Squartini S, Zaman F, Muttaqi KM. Energy management of community microgrids considering degradation cost of battery. J Energy Storage 2019;22:257–69.
- [25] Twidell J. Renewable energy resources. Routledge; 2021.
- [26] Hossain MA, Pota HR, Issa W, Hossain MJ. Overview of AC microgrid controls with inverter-interfaced generations. Energies 2017;10(9):1300.